Zonal variations of peak ionization rates in upper atmosphere of Mars at high latitude using Mars Global Surveyor accelerometer data

S. P. Seth,[1,2] V. Brahmananda Rao,[1] C. M. Esprito Santo,[1] S. A. Haider,[3] and V. R. Choksi[3]

[1]   The Accelerometer Experiment onboard Mars Global Surveyor (MGS) measured many density profiles in the upper atmosphere of Mars during aerobraking at many latitudes, longitudes, altitudes, local solar time (LST), and seasons. Here, in this paper, we use the accelerometer data of 57 orbits (P0588–P0648) from 30 September 1998 to 24 October 1998 between latitude ranges (50°–70°N) at LST 1600 hours, under spring equinox and medium solar activity conditions (average $F_{10.7} \sim 120$). Using these densities, the neutral densities of different gases are derived from their mixing ratio. From these neutral densities the longitudinal distribution of peak photoionization rates, peak photoelectron impact ionization rates, and the total peak ionization rates of CO_2^+, N_2^+ and O^+ are obtained for solar zenith angle 78° at wavelength range 10–1025.7 Å due to solar EUV radiation using analytical yield spectrum approach (AYS). These calculations are made at different altitudes and longitudes starting from 115 to 220 km and 0° to 360°E using intervals of 0.1 km and 5°, respectively. These conditions are appropriate for MGS phase 2 aerobraking period from which the accelerometer data are used. The Fourier analysis of the various peak ionization rates of CO_2^+, N_2^+, and O^+ indicates the presence of two dominant harmonic regions at high latitude in the upper atmosphere of Mars. The first is a class of long planetary-scale waves that may be associated with the fixed topography of Martian surface. The second is a class of rapidly moving transient disturbances that may be associated with baroclinic instability processes.

1.   Introduction

[2]   Mars Global Surveyor (MGS) was launched in November 1996 and reached Mars in September 1997. The orbit of MGS was altered using the technique of aerobraking. Aerobraking took place in two phases, 1 and 2, separated by a hiatus containing the Science Phasing Orbits [*Albee et al.*, 1998, 2001]. The orbit of MGS during aerobraking was near polar and highly elliptical, with an inclination of about 93°. During the aerobraking phase, many observations were carried out by the various instruments onboard MGS [*Albee et al.*, 2001].

[3]   The Accelerometer Experiment onboard MGS measured many density profiles in the upper atmosphere of Mars during aerobraking at many latitudes, longitudes, altitudes, local solar time (LST) and seasons [*Withers et al.*, 2003]. Aerobraking took place in two phases, 1 and 2.

Phase1 included the orbits from P1-P201 from mid September 1997, to late March 1998, while phase 2 included the orbits from P574-P1283 from mid September 1998, to early February 1999. The maximum altitude at which the accelerometer measured thermospheric density as set by the sensitivity of the instrument was 160 km. The minimum altitude at which it measured the thermospheric density was that of periapsis, which is rarely outside 100–120 km. The MGS accelerometer data have been used for studies of global features and dynamical properties of neutral atmosphere [*Keating et al.*, 1998; *Tolson et al.*, 1999; *Bougher et al.*, 2001, 2004; *Withers et al.*, 2003; *Withers*, 2006]. The analysis of these aerobraking data sets confirms a strong coupling of the lower and upper atmosphere of Mars [*Bougher et al.*, 2006, and references therein].

[4]   In a Fourier analysis for the kinetic energy of meridional wind in Earth's lower atmosphere, *White and Cooley* [1956] obtained two regions of maximum kinetic energy, one in the lower wave number around 4 and the other around 8. They attributed these two maxima respectively to the fixed topography [*Charney and Eliassen*, 1949], heat sources and sinks [*Smagorinsky*, 1953] and to the baroclinic instability process [*Charney*, 1947].

[5]   The behavior of Martian atmosphere is similarly represented by forced and free oscillations. The forced

---

[1]Instituto Nacional de Pesquisais Espaciais, Sao Jose dos Campos, Brazil.
[2]Bhavan's R.A. College of Science, Gujarat University, Ahmedabad, India.
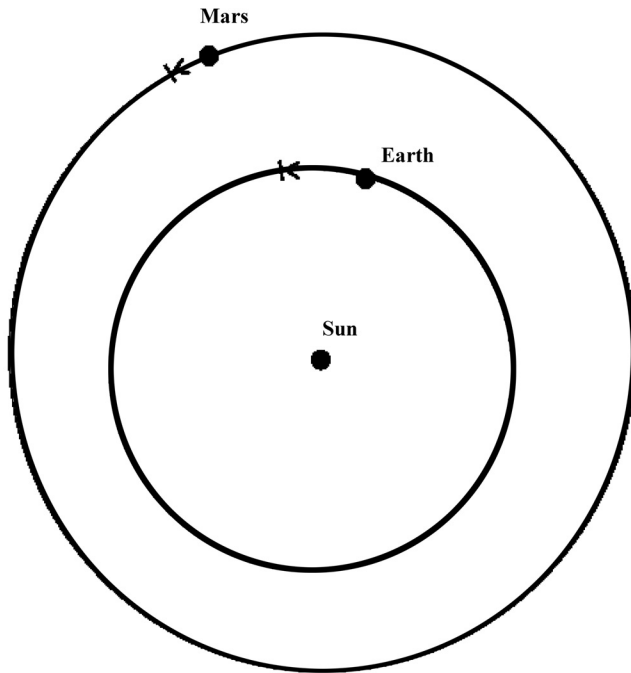[3]Physical Research Laboratory, Ahmedabad, India.

Figure 1. Geometry of Sun, Earth, and Mars during the period 30 September 1998 to 24 October 1998. The solid dots give the position of Earth and Mars on 30 September, and the thin solid lines give their positions on 24 October.

oscillations are the atmosphere's response to the daily cycle of Sun, or spatial differences in the heating and topography while the free oscillations include atmospheric instabilities. On Earth, the forced oscillations are mainly due to stationary waves which are induced by topography and ocean-continent heating differences. They have a strong control over the weather, and thus are important to our everyday lives. Similarly, on Mars, the forced oscillations are important not only through a possible influence on the weather, but also by contributing in a significant way to overall distribution of heat on the planet. The forced oscillations consist of thermal tides and stationary waves. The thermal tides are relatively strong on Mars compared to the Earth [*Banfield et al.*, 2003, and references therein]. The thermal tides consist not only of modes that follow the Sun (so-called migrating tides), but also, through their interaction with topography they have modes which do not follow the Sun, called as nonmigrating tides. These nonmigrating tides are expected to exert their strongest influence in the upper atmosphere, modulating the atmospheric density at ~130 km and hence the aerobraking experienced by orbiters [*Forbes and Hagan*, 2000; *Wilson*, 2000, 2002]. The stationary waves can influence the stability of the atmosphere, enhancing the formation of free disturbances at certain longitudes and impeding their formation at others [*Hollingsworth and Barnes*, 1996].

[6] This paper has two objectives: (1) Using accelerometer data of 57 orbits (P0588–P0648) between latitude ranges (50°–70°N) from 30 September 1998 to 24 October 1998, under spring equinox and medium solar activity conditions (average $F_{10.7} \sim 120$) during phase 2 of the aerobraking, we calculate the longitudinal distributions of

peak photoionization rates, peak photoelectron impact ionization rates, total peak ionization (photoionization + photoelectron impact ionization) rates in the upper atmosphere of Mars. During these orbits, the Martian heliocentric longitude L_s is from 34° to 45°, solar zenith angle (SZA) is from 56° to 66° and local solar time (LST) is 1600 hours. The calculations of these peak ionization rates are carried out at different altitudes and longitudes starting from 115 km to 220 km and from 0°E to 360°E at the intervals of 0.1 km and 5° respectively for solar zenith angle 78° due to absorption of solar EUV radiation (10–1025.7 Å) using analytical yield spectrum (AYS) approach. (2) The peak ionization rates exhibit wave nature in the same way as the measured mass density does. By performing the Fourier analysis of these peak ionization rates we therefore obtain the dominant harmonics prevalent in the various ionization rates of CO_2^+, N_2^+ and O^+ in the upper atmosphere of Mars.

2. Longitudinal Distribution of Ionization Rates
2.1. Photoionization Production Rates

[7] The longitudinal distribution of photoelectron spectra due to absorption of solar EUV radiation (10–1025.7 Å) are calculated using formula given below:

$$Q(Z, \Psi, E) = \sum_i n_i(Z, \Psi) \sum_\lambda \sigma_i^I(\lambda) I(\infty, \lambda) \delta\left(\frac{hc}{\lambda} - E - W_i\right)$$

$$\cdot \exp\left[-\sum_i \sigma_i^A(\lambda) \int_Z^\infty n_i(Z, \Psi) Ch(X, \chi) dZ\right] \quad (1)$$

where $\sigma_i^I(\lambda)$ and $\sigma_i^A(\lambda)$ are respectively the photoionization and photoabsorption cross sections of gas i at wavelength λ, $n_i(Z,\Psi)$ is neutral density of gas i at altitude Z and longitude Ψ; $I(\infty, \lambda)$ is the incident solar photon flux at the top of Martian atmosphere; $\delta(\frac{hc}{\lambda} - E - W_i)$ is the delta function in which $\frac{hc}{\lambda}$ is incident photon energy; W_i is the ionization potential of ith constituent and E is the energy of ejected electron. It is assumed that electrons are ejected isotropically. The function $Ch(X, \chi)$ is called Chapman's grazing incidence [*Smith and Smith*, 1972] and takes into account the absorption of the solar radiation as it passes obliquely through the atmosphere. This function depends on the solar zenith angle χ and a dimensionless parameter $X = (R_M + Z_o)/H$, where R_M is the radius of Mars and H is scale height of the neutral atmosphere. The primary photoelectron distributions due to absorption of solar EUV radiation (10–1025.7 Å) are calculated at solar zenith angle 78° under solar moderate condition.

[8] The mass density from accelerometer experiment, between latitude (50°–70°N), for the orbits P0588 to P0648 (57 orbits) from 30 September 1998 to 24 October 1998 during early northern spring is available only from 115 km and up to 160 km. No model exists which can calculate the neutral density incorporating simultaneously all the necessary physical processes of the Martian atmosphere at various latitude, longitude, season and local solar time. Therefore the neutral densities of five gases namely CO_2, N_2, O_2, O and CO are derived from 115 km to 160 km and from 0° E to 360° E at the interval of
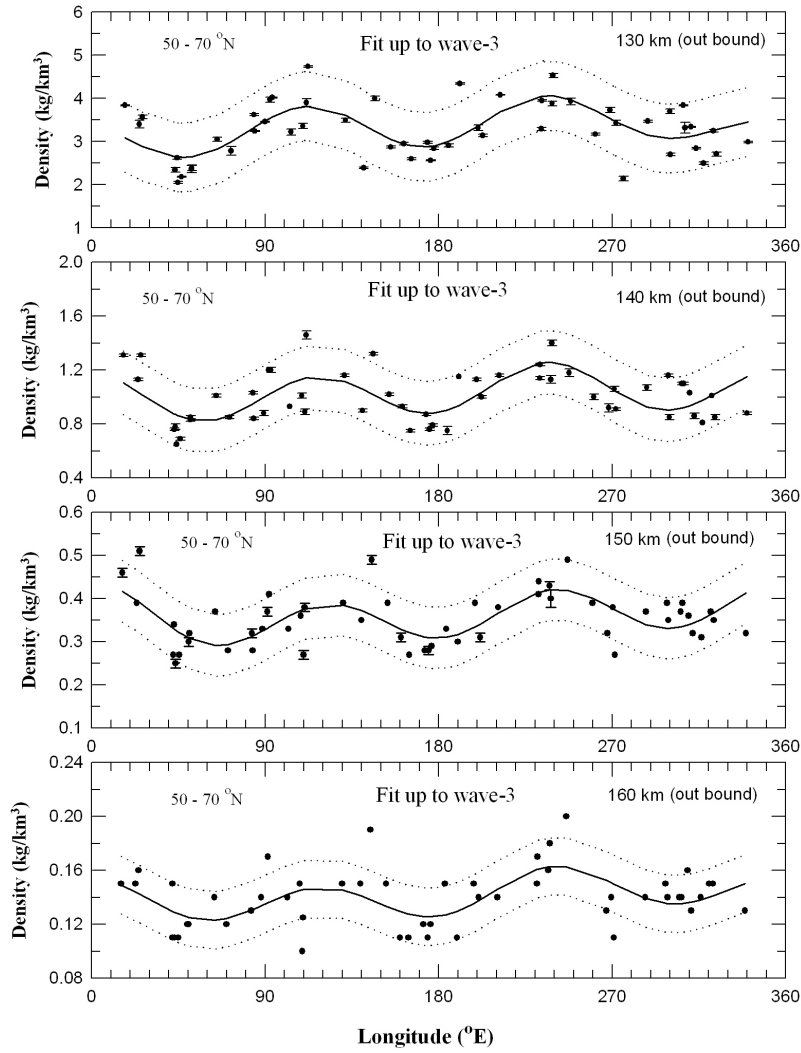
Figure 2. MGS accelerometer data of mass density for latitude range $50°-70°N$ from altitudes 130 km and 160 km along with measurement uncertainties. Solid line indicates best fit to data, and dotted lines represent 0.95 confidence limits.

0.1 km and 5° respectively by multiplying the mixing ratios of these gases with the mass densities. The linear interpolation method is used wherever accelerometer data is not available at these intervals. The mixing ratios are adopted from *Bougher et al.* [2000] and *Fox* [1997] at different altitudes for similar conditions of MGS phase 2 aerobraking period. The accelerometer experiment measured the mass density up to 160 km. Above 160 km and up to 220 km the neutral densities are taken from *Bougher et al.* [2000].

[9] The branching ratios, photoabsorption and photoionization cross sections are taken from other references [e.g., *Raina and Haider*, 1998; *Haider et al.*, 2002; *Seth*, 2003]. The solar flux is taken from SOLAR 2000 model [*Tobiska et al.*, 2000] which is an empirical model of the full solar spectrum drawing ground-based and satellite measurements available for each day. The solar flux is scaled by $1/R^2$ where R is heliocentric distance equal to 1.644 AU, appropriate for accelerometer experiment for the above mentioned period during MGS phase 2 aerobraking period.

The photoionization rates are obtained by integrating equation (1) over energy.

2.2. Photoelectron Impact Production Rates

[10] The longitudinal distribution of Photoelectron impact production rates are obtained in the dayside ionosphere of Mars using two dimensional AYS approach as described by *Haider and Bhardwaj* [2005] and *Seth* [2003]. This approach is useful in the lower thermosphere ($\sim$220 km), where the vertical transport of photoelectron is not allowed. Thus the photoelectrons produced after photon impact ionization loose their energy at the same height where they are produced. Using AYS approach, the Photoelectron impact production rates are calculated as given below:

$$R_i(Z, \Psi) = \int\limits_{W_i}^{\infty} \int\limits_{E}^{\infty} Q(Z, \Psi, E) u^c(E, E_o) p_i(E) dE dE_o \quad (2)$$

$$p_i(E) = C_i \left(1 - \in_i^{-\alpha_i}\right)^{\gamma_i} \in_i^{-u_i} \quad (3)$$
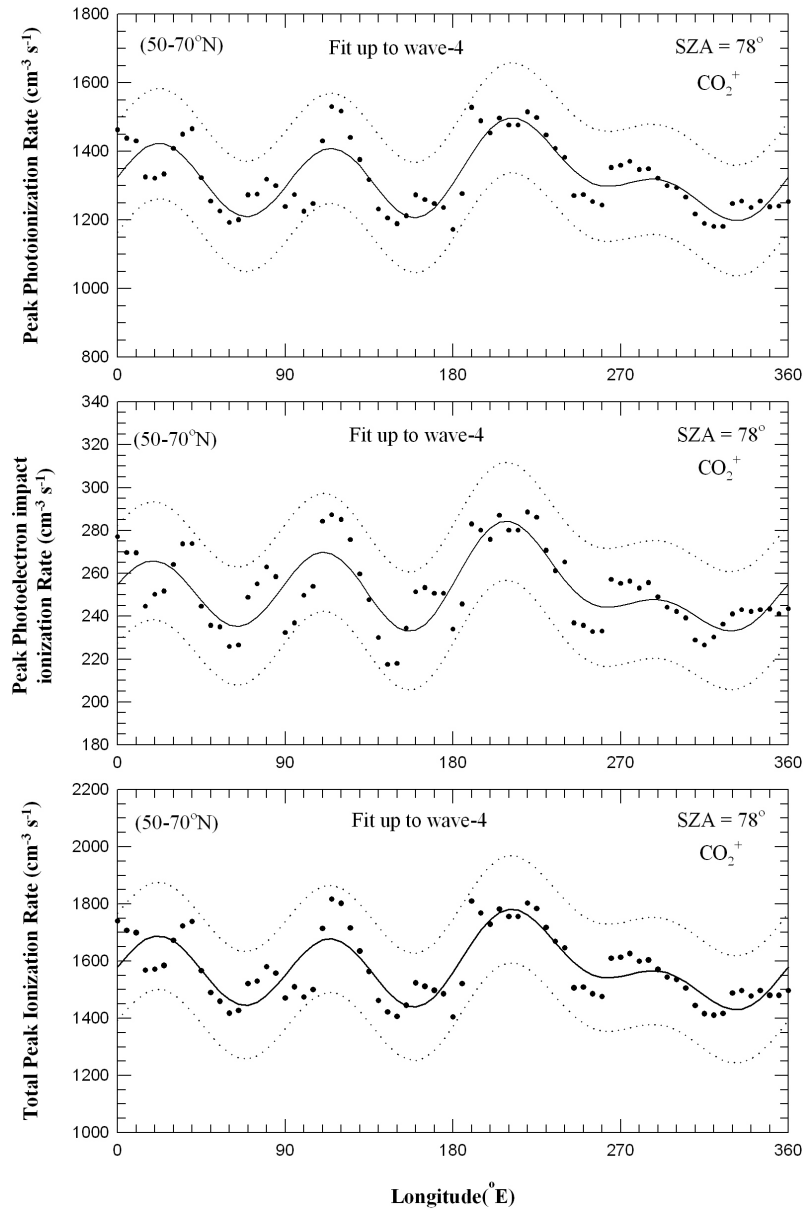
Figure 3. Longitudinal variation of peak photoionization rates, peak photoelectron impact ionization rates, and total impact ionization rates of CO_2^+ between latitude range 50° and 70°N. Solid line indicates the best fit to data, and dotted lines represent 0.95 confidence limits.

where $R_i(Z, \Psi)$ is the ion production rates at altitude Z and longitude Ψ; $p_i(E)$ is ionization probability; $\in_i = E/I_i$, I_i being lowest ionization threshold. The parameters C_i, α_i, γ_i and u_i in equation (3) are taken from *Haider* [1999] for different gases in the atmosphere of Mars, $Q(Z, \Psi, E)$ is the primary photoelectron spectra, $u^c(E,E_o)$ is two dimensional composite yield spectra at energy E_o and E. Here E_o is the incident energy of monoenergetic electrons introduced in a gas medium of gas and E is the energy of secondary or tertiary electrons, which were calculated when the primary electrons ionize the atmospheric constituents. For a mixture of gas, the composite yield spectra $u^c(E,E_o)$ are obtained by weighting the component of yield spectra as described by *Seth et al.* [2002]. To save the computational time for the calculation of photoelectron impact ion-

ization rates, the energy grids of width 2 eV between 0 and 10 eV and a width of 2.5 eV between 10 and 1000 eV is chosen.

3. Fourier Analysis of Peak Ionization Rates

[11] The amplitudes of the components of harmonic of peak ionization rates (I) from 0° E to 360° E at 5° interval are given by

$$a_n = \frac{1}{L} \int_o^L I(x) \cos\left[\frac{2\pi nx}{L}\right] dx \approx \frac{1}{72} \sum_{j=1}^{72} I(x) \cos\left[\frac{2\pi nj}{72}\right] \quad (4)$$

$$b_n = \frac{1}{L} \int_o^L I(x) \sin\left[\frac{2\pi nx}{L}\right] dx \approx \frac{1}{72} \sum_{j=1}^{72} I(x) \sin\left[\frac{2\pi nj}{72}\right] \quad (5)$$
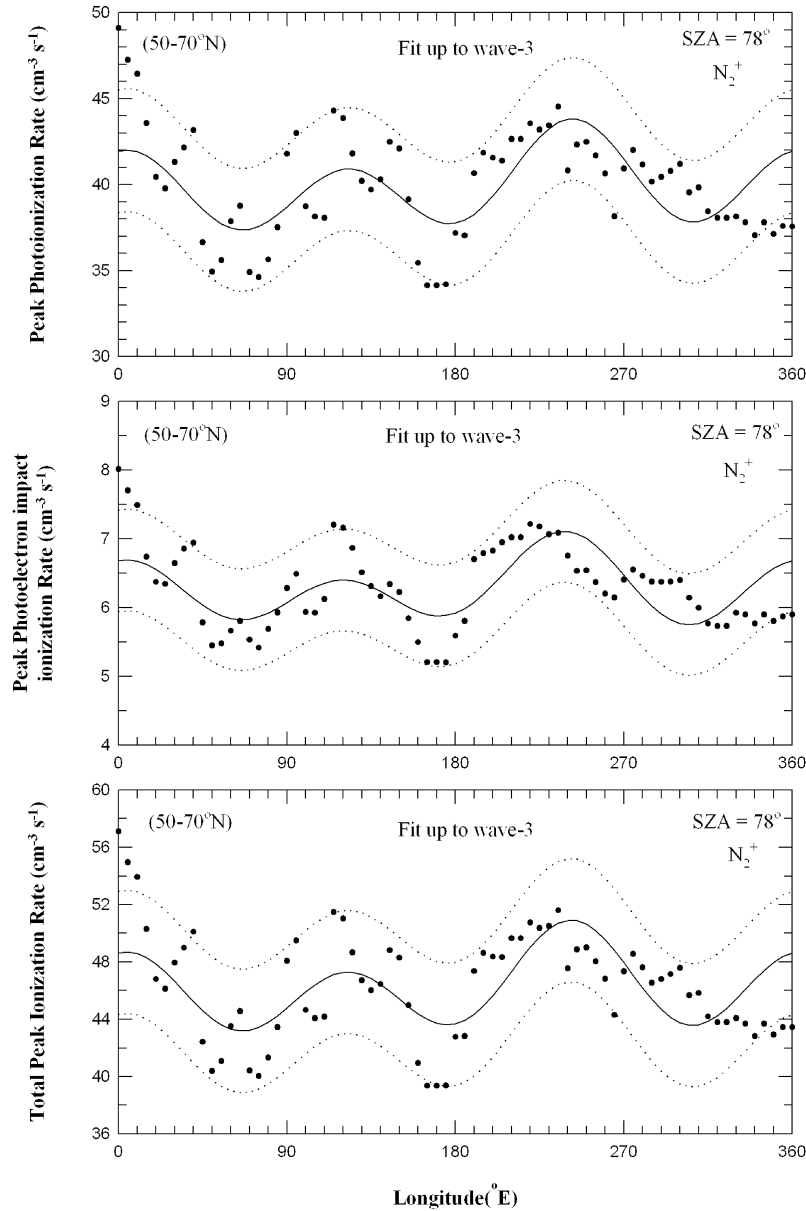
Figure 4. Longitudinal variation of peak photoionization rates, peak photoelectron impact ionization rates, and total impact ionization rates of N_2^+ between latitude range $50°$ and $70°N$. Solid line indicates the best fit to data, and dotted lines represent 0.95 confidence limits.

$$I = A_n \sin(Kx + \delta) \qquad (6)$$

where $A_n = \sqrt{a_n^2 + b_n^2}$ and $\tan \delta = \dfrac{b_n}{a_n}$.

Here a_n and b_n are the amplitudes of the components of the harmonics of peak photoionization and peak photoelectron impact ionization rates evaluated at 72 equally spaced longitudinal points. It has been shown by *Whittaker and Robinson* [1967] that the values of a_n and b_n as obtained above are also the least squares fit of the harmonics. We also propose to calculate the contribution of each harmonic due to peak photionization and peak electron impact ionization rates for the total variance. If D is the zonal distribution of peak ionization rate then $D = \overline{D} + D'$ where $\overline{D}$ is the zonal mean and D' is the deviation. The Variance V is given as

$V = \overline{D'^2}$. The contribution of each harmonic is $A_n^2/2$. Thus the percentage variance explained by harmonic n is $\left[\dfrac{A_n^2/2}{V}\right]$.

4. Results and Discussion

[12] Figure 1 shows the orbital positions of Earth and Mars for the period 30 September 1998 to 24 October 1998. The Earth-Sun-Mars angle was $-115°$ on 30 September 1998 and it decreases monotonically to $-103°$ on 24 October 1998. Here we adopt the convention that Earth-Sun-Mars angles are negative, when the Earth is trailing Mars (i.e., prior to opposition) and positive when Mars is trailing Earth (i.e., after opposition).
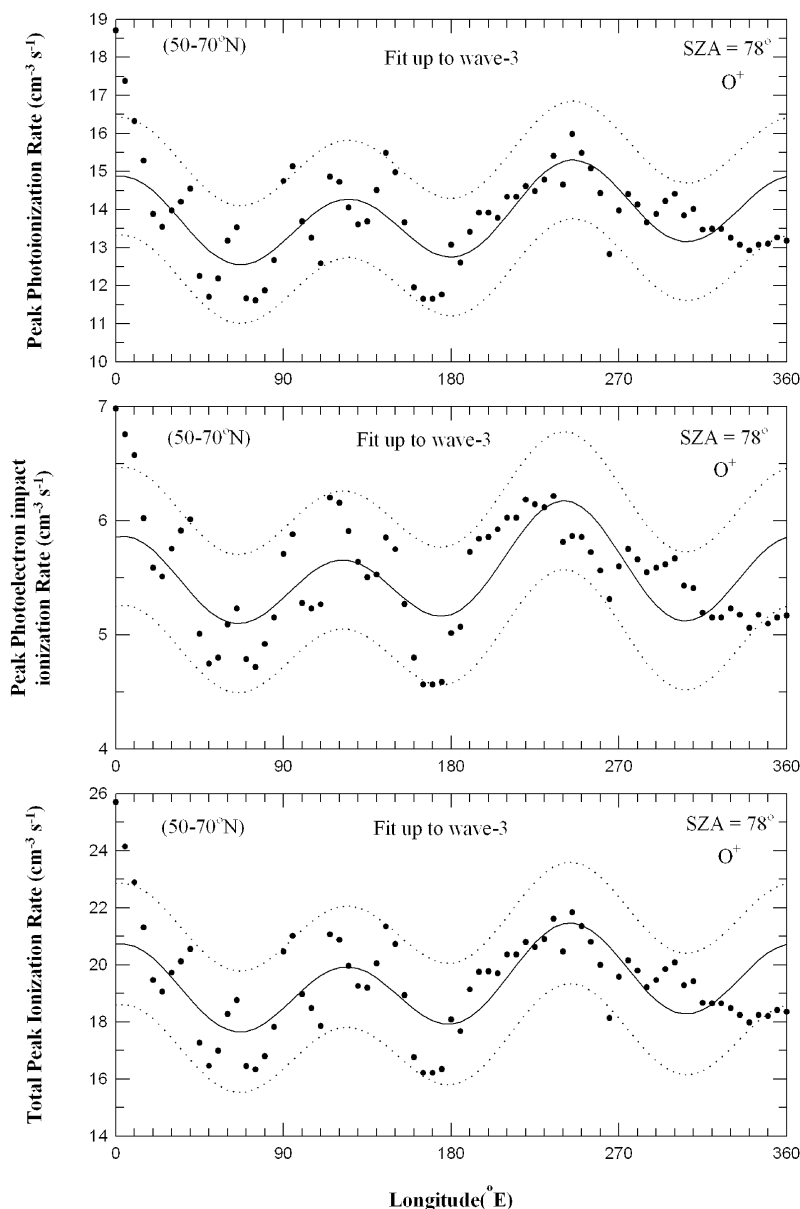
Figure 5. Longitudinal variation of peak photoionization rates, peak photoelectron impact ionization rates, and total impact ionization rates of O^+ between latitude range $50°$ and $70°N$. Solid line indicates the best fit to data, and dotted lines represent 0.95 confidence limits.

[13] Figure 2 represents the distribution of mass density at reference altitudes of 130, 140, 150 and 160 km versus longitude for the outbound leg of orbits P0588–P0648 measured by MGS accelerometer experiment from 30 September 1998 to 24 October 1998. Initially, *Keating et al.* [1998] suggested that this zonal variation is due to topographically forced stationary waves. However, later it has been shown that this is due to the presence of thermal tides [*Keating et al.*, 2001; *Forbes and Hagan*, 2000; *Joshi et al.*, 2000; *Wilson*, 2002]. Thermal tides are planetary-scale waves with periods that are harmonics of the solar day. These include westward propagating, migrating (Sun synchronous) waves forced in response to solar heating, and additional nonmigrating waves resulting from the zonal variations in the thermotidal forcing. *Wilson* [2000] showed

that the longitudinal variability of both midlevel ($\sim$25 km) morning and afternoon temperatures derived from MGS Thermal Emission Spectrometer (TES) spectra is dominated by nonmigrating tides. The model results indicate that these tides can propagate from the lower atmosphere into the thermosphere [*Forbes and Hagan*, 2000; *Wilson*, 2000]. Thus the mass density measurements indicate the presence of planetary-scale wave structure and tidal waves in the upper atmosphere of Mars [*Hinson et al.*, 2001; *Wilson*, 2002]. These types of waves arise in response to surface forcing [e.g., *Hollingsworth and Barnes*, 1996; *Barnes et al.*, 1996; *Nayvelt et al.*, 1997; *Wilson and Richardson*, 2000]. During these orbits, the Martian heliocentric longitude L_s is from $34°$ to $45°$, solar zenith angle (SZA) is from $56°$ to $66°$ and local solar time (LST) is 1600 hours. During

Table 1. Peak Altitudes and Peak Production Rates due to Photoionization and Electron Impact Ionization for Medium Solar Activity

Species	Photoionization		Electron Impact Ionization	
	Peak Altitude, km	Peak Production Rate, $cm^{-3} s^{-1}$	Peak Altitude, km	Peak Production Rate, $cm^{-3} s^{-1}$
CO_2^+	$137-145$	$1179-1529$	$135-143$	$217.40-288.50$
N_2^+	$144-154$	$34.13-49.10$	$141-150$	$5.20-8.00$
O^+	$144-157$	$11.61-18.71$	$142-154$	$4.56-6.98$

this time period the dust storm activity was minimum. The outbound orbit provides more data points than that obtained during inbound orbits. Therefore we have taken density in our model from various outbound orbits. The following fundamental equation is used by *Keating et al.* [1998], to derive mass density from MGS accelerometer experiment:

$$\rho = \frac{2ma}{v^2 C_D s} \quad (7)$$

where v is spacecraft velocity vector, a is drag force acceleration, ρ is atmospheric mass density, m is mass of spacecraft, s is cross sectional area relative to v and C_D is drag coefficient.

[14] The characteristics of mass density and various peak ionization rates as a function of longitude Ψ in the upper atmosphere of Mars are assumed to be approximated by a wave k model as follows:

$$y = a_0 + a_1 \cos(\psi) + b_1 \sin(\psi) + \cdots \cdot a_k \cos(k\psi) + b_k \sin(k\psi) \quad (8)$$

where y is either mass density or various peak ionization rates, Ψ is east longitude, and the a_i and b_i are model parameters, which are calculated by minimizing chi square. This approach is similar to the approximation used by *Withers et al.* [2003], *Krymskii et al.* [2003] and *Bougher et al.* [2001] for studying the longitudinal variations in the thermosphere/ionosphere of Mars. We have employed above equation for the least squares spectral fitting to the mass density and various peak ionization rates in the upper atmosphere of Mars.

[15] Measurement uncertainties are also shown in Figure 2, which are much smaller than the range in multiple measurements at any longitude. We use a least squares fit up to wave 3 (wave 1, 2, plus 3) harmonic model to characterize the zonal structure as shown in Figure 2 [*Withers et al.*, 2003; *Krymskii et al.*, 2003, *Bougher et al.*, 2001]. This model contains a constant density term, an amplitude and phase for a sinusoid with one cycle per 360° of longitude, which is labeled as wave 1 harmonic, and higher harmonics up to and including wave 3. It has seven free parameters. In Figure 2 the solid and dotted lines are plotted for model fit values and 0.95 confidence limit respectively. The zonal structure with large peaks in density at ∼110°−120° E and ∼230°−240°E can be seen. Also, it can be seen from Figure 2 that the zonal structure which is present between 130 and 160 km, decays with increasing altitude.

[16] The longitudinal distribution of peak photoionization, peak photoelectron impact ionization and the total peak ionization of three major ions: CO_2^+, N_2^+ and O^+ at SZA = 78° caused by solar EUV radiation (10−1025.7 Å) are shown in Figures 3, 4, and 5 at different east longitudes. In Table 1 the summaries of the peak altitudes, the magnitudes of peak photoionization rates and peak electron

impact ionization rates for the three major ions CO_2^+, N_2^+ and O^+ are presented. The main peaks in the production profiles are due mostly to absorption of the portion of EUV from 250 to 910 Å. The major ion produced is CO_2^+ and its production rate due to photoionization and electron impact ionization maximizes from 137−145 km, 135−143 km for the various longitudes. Similarly the production rate of N_2^+ and O^+ due to photoionization and electron impact ionization maximizes from 144−154 km, 141−150 km and from 144−157 km, 142−154 km for the various longitudes. The magnitudes of peak photoionization, peak photoelectron impact ionization of CO_2^+, N_2^+ and O^+ are ∼1179−1529 $cm^{-3} s^{-1}$, 217.4−288.5 $cm^{-3} s^{-1}$; 34.13−49.10 $cm^{-3} s^{-1}$, 5.20−8.00 $cm^{-3} s^{-1}$; 11.61−18.71, 4.56−6.98 $cm^{-3} s^{-1}$. As it is seen from Figure 3 that peak photoionization, peak photoelectron impact ionization and the total peak ionization of CO_2^+ is fitted with a harmonic up to wave 4 (wave 1, 2, 3, plus 4) harmonic model which has 9 free parameters. Similarly the peak photoionization, peak photoelectron impact ionization and the total peak ionization of N_2^+ and O^+ is fitted with a harmonic up to wave 3 (wave 1, 2, plus 3) harmonic model which has 7 free parameters. The solid and dotted lines are plotted for model fit values and 0.95 confidence limit respectively.

[17] To explain the dominance of harmonics up to and including wave 4 (wave 1, 2, 3, plus 4) in various peak ionization rates of CO_2^+ and the dominance of harmonics up to and including wave 3 (wave 1, 2, plus 3) in various peak ionization rates of N_2^+ and O^+, we perform the Fourier analysis of various peak ionization rates as explained in

Table 2. Percentage of Variance as Explained by Individual Harmonics for CO_2^+, N_2^+ and O^+

| Wave	Peak Photoionization			Peak Electron Impact Ionization		
	CO_2^+	N_2^+	O^+	CO_2^+	N_2^+	O^+
1	5.38	4.93	6.81	6.26	4.70	4.85
2	14.36	2.39	0.46	11.39	6.83	3.93
3	10.16	28.59	31.64	11.42	28.78	30.27
4	33.83	18.54	5.55	27.86	26.39	20.95
5	3.98	4.64	5.90	2.05	4.45	4.92
6	0.46	1.87	3.84	2.38	0.98	1.90
7	1.94	1.72	5.32	5.40	0.26	1.20
8	1.45	3.40	5.55	3.80	0.87	2.28
9	9.76	1.41	0.93	11.33	3.56	2.04
10	5.54	2.86	2.47	3.51	3.53	3.26
11	1.73	0.65	0.42	3.40	1.13	0.74
12	0.98	9.40	10.71	0.38	6.41	8.25
13	1.80	8.01	7.16	1.53	4.42	6.48
14	1.43	1.56	1.32	1.26	0.72	1.02
15	0.46	0.01	0.02	0.32	0.05	0.01
16	0.11	0.42	0.57	0.13	0.29	0.32
17	0.04	0.61	0.71	0.06	0.23	0.38
18	0.12	0.49	0.71	0.05	0.16	0.20
19	1.09	0.98	0.79	0.84	0.78	0.73
20	0.15	0.74	0.83	0.02	0.43	0.66
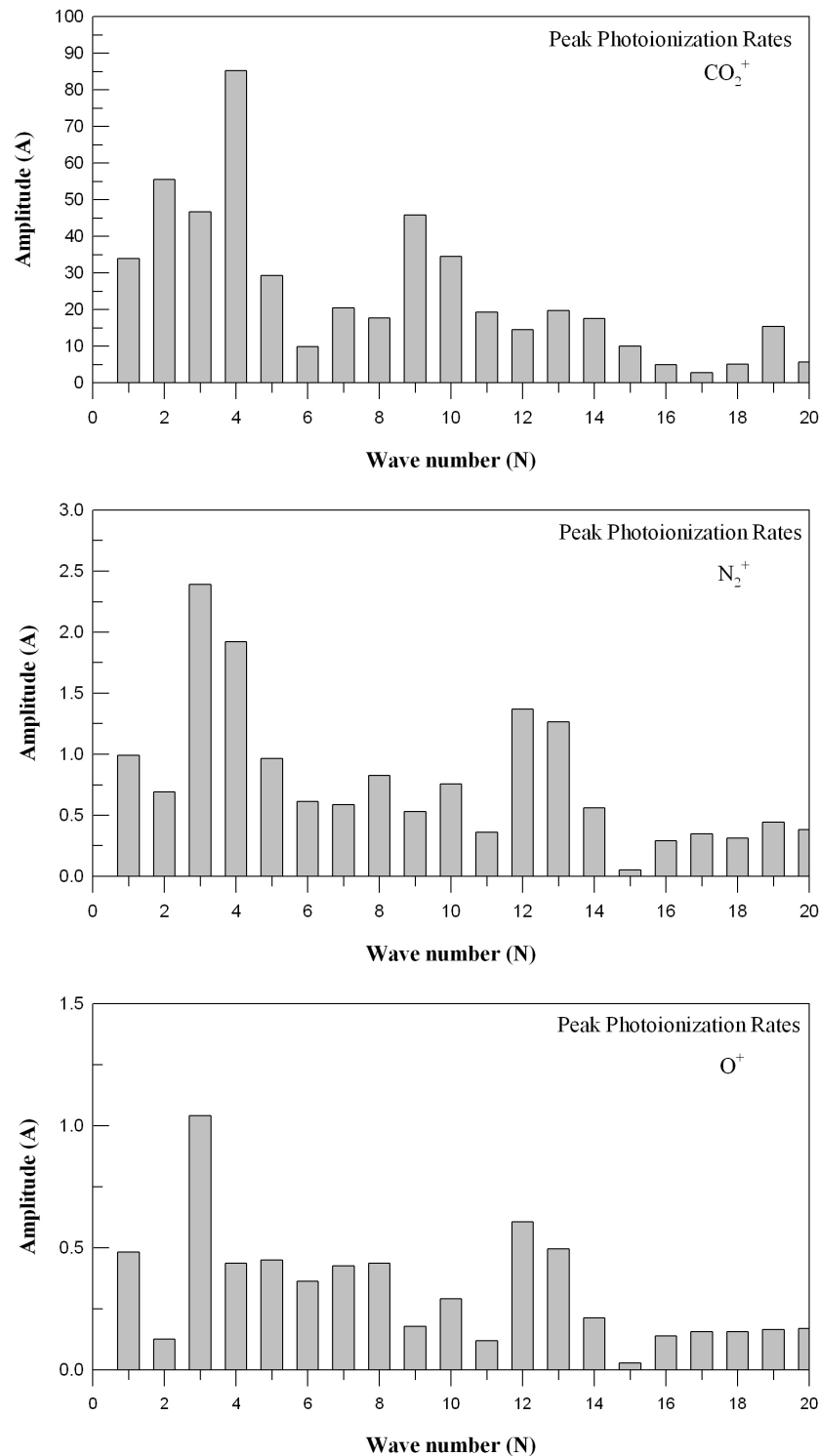
Figure 6. Distribution of amplitude and wave numbers due to peak photoionization rate spectra of CO_2^+, N_2^+, and O^+ in the upper atmosphere of Mars.

section 3. In this analysis, we have calculated the percentage of variance as explained by individual harmonics for CO_2^+, N_2^+ and O^+ due to peak photoionization and peak photoelectron impact ionization rate as shown in Table 2.

[18] It is clear from Figures 6 and 7 and Table 2 that the most pronounced feature of the peak photoionization and peak photoelectron impact ionization rates spectra of CO_2^+, N_2^+ and O^+ are that, at least two maxima always exist. This indicates the presence of two prominent and distinct wave numbers in the various peak ionization rates of CO_2^+, N_2^+ and O^+ prevalent in the ionosphere of Mars at high latitude. The first is a class of long planetary-scale waves which contribute to the high frequency of disturbances with maximum amplitude at about wave number 4 for CO_2^+
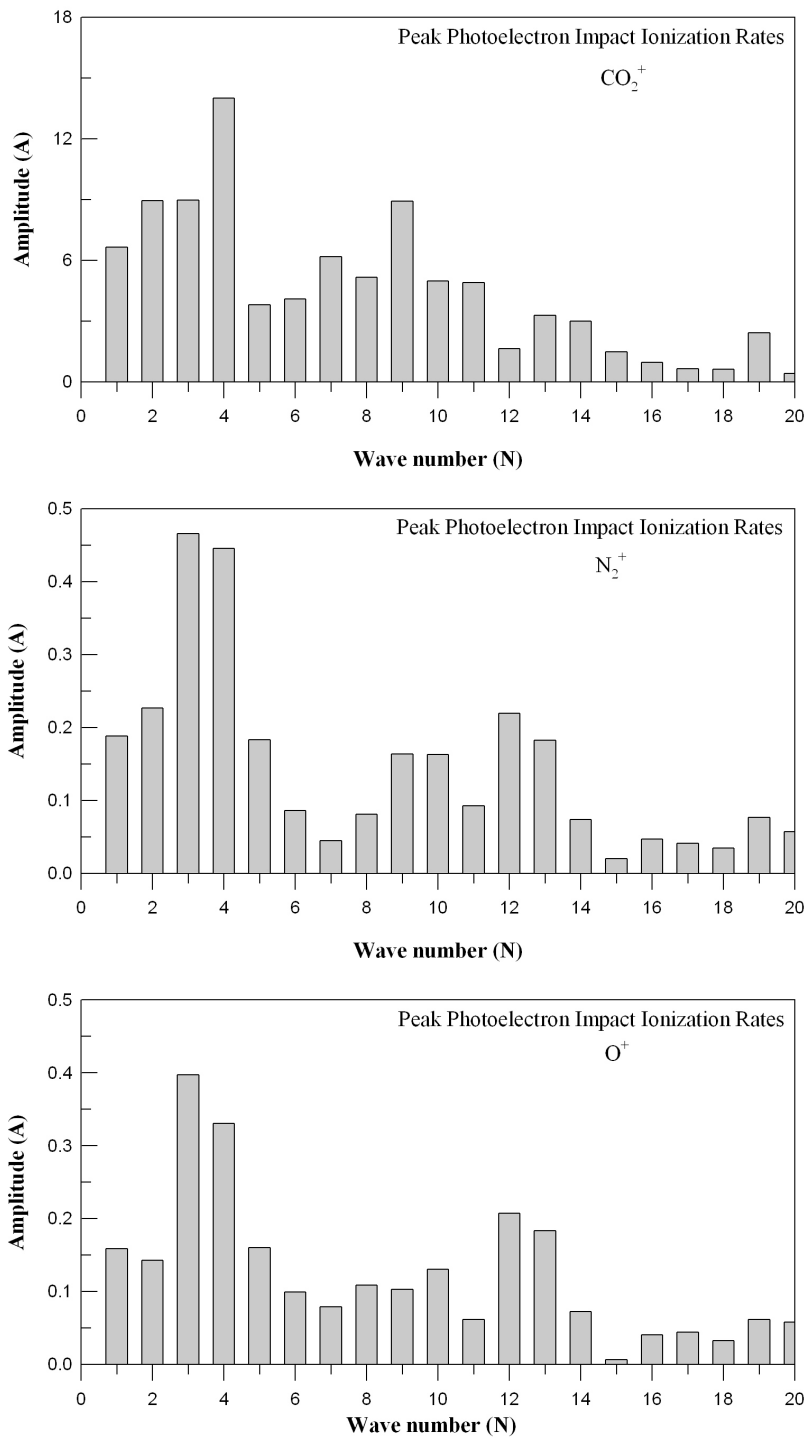
Figure 7. Distribution of amplitude and wave numbers due to peak photoelectron impact ionization rate spectra of CO_2^+, N_2^+, and O^+ in the upper atmosphere of Mars.

and at wave number 3 for N_2^+ and O^+. These disturbances may be associated with the fixed topography of Martian surface. The second is a class of rapidly moving transient disturbances clustered around wave number 9 for CO_2^+ and around wave number 12–13 for N_2^+ and O^+. These disturbances may be associated with baroclinic instability processes. These two types of waves are probably generated in the lower atmosphere of Mars and propagate to the upper atmosphere of Mars due to strong coupling of

the lower and upper atmosphere of Mars as mentioned by various investigators [*Bougher et al.*, 2006, and the references therein].

5. Conclusions

[19] Using the density profiles of the Mars upper atmosphere, measured with the accelerometer of MGS, the longitudinal distribution of peak photoionization rates, peak

photoelectron impact ionization rates and their total peak ionization rates are obtained for solar zenith angle 78° at wavelength range $10-1025.7$ Å due to solar EUV radiation using analytical yield spectrum approach (AYS). Initially these zonal variations were attributed due to topographically forced stationary waves. However, later it has been shown that this is due to the presence of thermal tides which are planetary scale waves. These tides can propagate from the lower atmosphere into the thermosphere. The subsequent Fourier analysis of the various calculated peak ionization rates indicates the presence of two distinct harmonics in the upper atmosphere of Mars. The first is a class of long planetary-scale waves which contribute to the high frequency of disturbances with maximum amplitude at about wave number 4 for CO_2^+ and at wave number 3 for N_2^+ and O^+. These disturbances may be associated with the fixed topography of Martian surface. The second is a class of rapidly moving transient disturbances clustered around wave number 9 for CO_2^+ and around wave number $12-13$ for N_2^+ and O^+ which may be associated with baroclinic instability processes.

References

Albee, A. L., F. Palluconi, and R. E. Arvidson (1998), Mars Global Surveyor mission: Overview and status, *Science*, *279*, 1671.

Albee, A. L., R. E. Arvidson, F. Palluconi, and T. Thorpe (2001), Overview of Mars Global Surveyor mission, *J. Geophys. Res.*, *106*, 23,291.

Banfield, D., B. J. Conrath, M. D. Smith, P. R. Christensen, and R. J. Wilson (2003), Forced waves in the Martian atmosphere from MGS TES nadir data, *Icarus*, *161*, 319.

Barnes, J. R., R. M. Haberle, J. B. Pollack, H. Lee, and J. Schaeffer (1996), Mars atmospheric dynamics as simulated by the NASA Ames General Circulation Model, 3, Winter quasistationary eddies, *J. Geophys. Res.*, *101*, 12,753.

Bougher, S. W., S. Engel, R. G. Roble, and B. Foster (2000), Comparative terrestrial planet thermospheres, 3, Solar cycle variation of global structure and winds at solstices, *J. Geophys. Res.*, *105*, 17,669.

Bougher, S. W., S. Engel, D. P. Hinson, and J. M. Forbes (2001), Mars Global Surveyor Radio Science electron density profiles: Neutral atmosphere implications, *Geophys. Res. Lett.*, *28*, 3091.

Bougher, S. W., S. Engel, D. P. Hinson, and J. R. Murphy (2004), MGS Radio Science electron density profiles: Interannual variability and implications for the Martian neutral atmosphere, *J. Geophys. Res.*, *109*, E03010, doi:10.1029/2003JE002154.

Bougher, S. W., J. M. Bell, J. R. Murphy, M. A. Lopez-Valverde, and P. G. Withers (2006), Polar warming in the Mars thermosphere: Seasonal variations owing to changing insolation and dust distributions, *Geophys. Res. Lett.*, *33*, L02203, doi:10.1029/2005GL024059.

Charney, J. G. (1947), The dynamics of long waves in a baroclinic westerly current, *J. Meteorol.*, *4*, 135.

Charney, J. G., and A. Eliassen (1949), A numerical method for predicting the perturbations of the middle latitude westerlies, *Tellus*, *1*, 38.

Forbes, J. M., and M. E. Hagan (2000), Diurnal Kelvin wave in the atmosphere of Mars: towards an understanding of "stationary" density structures observed by the MGS accelerometer, *Geophys. Res. Lett.*, *27*, 3563.

Fox, J. L. (1997), Upper limits to the outflow of ions at Mars: Implications for atmospheric evolution, *Geophys. Res. Lett.*, *24*, 2901.

Haider, S. A. (1999), Ionization and airglow in the Martian atmosphere, *Tech. Rep. ISRO-PRL-TR-100-99*, Phys. Res. Lab., Indian Space Res. Org., Ahmedabad.

Haider, S. A., and A. Bhardwaj (2005), Radial distribution of production rates, loss rates and densities corresponding to ion masses ≤40 amu in the inner coma of comet Halley: Composition and chemistry, *Icarus*, *177*, 196.

Haider, S. A., S. P. Seth, E. Kallio, and K. I. Oyama (2002), Solar EUV and electron-proton-hydrogen atom-produced ionosphere on Mars: Comparative studies of particle fluxes and ion production rates due to different processes, *Icarus*, *159*, 18.

Hinson, D. P., G. L. Tyler, J. L. Hollingsworth, and R. J. Wilson (2001), Radio occultation measurements of forced atmospheric waves on Mars, *J. Geophys. Res.*, *106*, 1463.

Hollingsworth, J. L., and J. R. Barnes (1996), Forced stationary planetary waves in Mars' winter atmosphere, *J. Atmos. Sci.*, *53*, 428.

Joshi, M. M., J. L. Hollingsworth, R. H. Haberle, and A. F. C. Bridger (2000), An interpretation of Martian thermospheric waves based on analysis of a general circulation model, *Geophys. Res. Lett.*, *27*, 613.

Keating, G. M., et al. (1998), The structure of the upper atmosphere of Mars: In-situ accelerometer measurements from Mars Global Surveyor, *Science*, *279*, 1672.

Keating, G. M., R. H. Tolson, A. M. Dwyer, S. W. Bougher, P. G. Withers, and J. M. Forbes (2001), Persistent planetary-scale wave-2 and wave-3 density variations observed in Mars upper atmosphere from MGS accelerometer experiment, paper presented at XXVI General Assembly, Eur. Geophys. Soc., Nice, France.

Krymskii, A. M., T. K. Breus, N. F. Ness, D. P. Hinson, and D. I. Bojkov (2003), Effects of crustal magnetic fields on the near terminator ionosphere at Mars: Composition of in situ magnetic field measurements with the data of radio science experiments on board Mars Global Surveyor, *J. Geophys. Res.*, *108*(A12), 1431, doi:10.1029/2002JA009662.

Nayvelt, L., P. J. Gierasch, and K. H. Cook (1997), Modeling and observations of Martian stationary waves, *J. Atmos. Sci.*, *54*, 986.

Raina, K. S., and S. A. Haider (1998), Chemistry of the dayside ionosphere of Mars, *Indian J. Radio Space Phys.*, *27*, 185.

Seth, S. P. (2003), Solar wind interaction with planets, Ph.D. thesis, Gujarat Univ., Ahmedabad, India.

Seth, S. P., S. A. Haider, and K. I. Oyama (2002), The photoelectron flux and nightglow emissions of 5577 A and 6300 A due to solar wind electron precipitation in Martian atmosphere, *J. Geophys. Res.*, *107*(A10), 1324, doi:10.1029/2001JA000261.

Smagorinsky, J. (1953), The dynamical influence of large scale heat sources and sinks on quasi-stationary mean motions of the atmosphere, *Q. J. R. Meteorol. Soc.*, *79*, 342.

Smith, F. L., and C. Smith (1972), Numerical evaluation of Chapman's grazing incidence integral Ch (χ, X), *J. Geophys. Res.*, *77*, 3592.

Tobiska, W. K., T. Woods, F. Eparvier, R. Viereck, L. Floyd, D. Bouwer, G. Rottman, and O. R. White (2000), The SOLAR 2000 empirical solar irradiance model and forecast tool, *J. Atmos. Sol. Terr. Phys.*, *62*, 1233.

Tolson, R. H., et al. (1999), Utilization of Mars Global Surveyor accelerometer data for atmospheric modeling, paper presented at Astrodynamics Specialist Conference, Am. Astrodyn. Soc., Girdwood, Alaska.

White, R. M., and D. S. Cooley (1956), Kinetic-energy spectrum of meridional motion in the mid-troposphere, *J. Meteorol.*, *13*, 67.

Whittaker, E., and G. Robinson (1967), The calculus of observations, 397 pp., Dover, Mineola, New York.

Wilson, R. J. (2000), Evidence for diurnal period Kelvin waves in the Martian atmosphere from Mars Global Surveyor TES data, *Geophys. Res. Lett.*, *27*, 3889.

Wilson, R. J. (2002), Evidence for nonmigrating thermal tides in the Mars upper atmosphere from the Mars Global Surveyor accelerometer experiment, *Geophys. Res. Lett.*, *29*(7), 1120, doi:10.1029/2001GL013975.

Wilson, R. J., and M. I. Richardson (2000), The Martian atmosphere during the Viking mission, 1, Infrared measurements of atmospheric temperatures revisited, *Icarus*, *145*, 555.

Withers, P. (2006), Mars Global Surveyor and Mars Odyssey accelerometer observations of the Martian upper atmosphere during aerobraking, *Geophys. Res. Lett.*, *33*, L02201, doi:10.1029/2005GL024447.

Withers, P., S. W. Bougher, and G. M. Keating (2003), The effects of topographically controlled thermal tides in the Martian upper atmosphere, *Icarus*, *164*, 14.

———————————

V. Brahmananda Rao, C. M. Esprito Santo, and S. P. Seth, INPE, 1758 Avenida dos Astronautas, Sao Jose dos Campos, SP 12201-970, Brazil. (sseth@das.inpe.br)

V. R. Choksi and S. A. Haider, Physical Research Laboratory, Ahmedabad 380 009, India.